QUALITY ASSESSMENT OF COMPRESSION TECHNIQUES FOR SYNTHETIC APERTURE RADAR IMAGES

Güner Arslan, Magesh Valliappan, and Brian L. Evans

Dept. of Electrical and Computer Engineering
The University of Texas at Austin, Austin, TX 78712-1084 USA
{arslan,magesh,bevans}@ece.utexas.edu

ABSTRACT

Synthetic aperture radar (SAR) systems are mounted on airplanes and satellites, which have limited downlink and storage capacity, yet SAR image sequences may be produced at rates of several Gbps. Compression is difficult because SAR images contain significant high-frequency information, such as terrain boundaries and terrain texture. In assessing the quality of compressed images, peak signal-to-noise ratio and mean-squared error are inadequate because they assume that distortion is solely due to image-independent additive noise. In this paper, we provide objective measures to assess the visual quality of SAR images compressed by JPEG and SPIHT coders. The human visual system responds differently to linear distortion and noise injection (nonlinear distortion plus additive noise). Our key contributions are that we (1) decouple and quantify the linear distortion and noise injection in JPEG and SPIHT coders, and (2) introduce a new edge correlation quality measure which we use to quantify nonlinear distortion.

1. INTRODUCTION

Synthetic Aperture Radar (SAR) is an active remote sensing system which has applications in agriculture, ecology, geology, oceanography, hydrology, and target recognition [1]. Compression techniques have been applied to SAR images because of limited storage and downlink capacity on mobile platforms. SAR images contain multiplicative speckle noise [1] and significant high-frequency information such as terrain boundaries and terrain texture [2]. Optical images contain a significant amount of low-frequency information because they are generally oversampled. Image compression techniques optimized for optical images may produce extremely undesirable artifacts for SAR images.

Quality measures are useful in evaluating the performance of compression techniques. As in optical images, mean squared error (MSE) and peak signal-to-noise ratio (PSNR) measures have been applied to SAR images [3, 4, 5]. Although these measures are simple to compute, they assume that the residual image (which is the difference between the decompressed and original images) is essentially independent noise. Unfortunately, compression degrades the original image by nonlinear distortion, linear distortion, and additive noise. Linear distortion causes the residual image to be correlated with the original image, which violates the assumption made by MSE and PSNR measures [6].

Other quality measures have been applied to block quantization, vector quantization, and discrete cosine transform compression for SAR images [2, 7]. Kuperman and Penrod [7] evaluate impulse response, contrast ratio, automatic target cueing, and image interpretability ratings. They find no significant statistical correlation between image quality and MSE or SNR measures. After evaluating 16 candidate measures, Dutkicwicz and Cumming [2] form a vector of seven relevant quality measures— data statistics, change in data histogram, error image, error image spectra, radiometric linearity, point target analysis, and MSE.

In this paper, we model an image coder as a linear filter plus noise injection to mimic the way that the human visual system (HVS) responds separately to these effects [6]. Noise injection includes nonlinear distortion and additive noise. Based on this model, we develop three quality measures for SAR images compressed by Joint Photographic Experts Group (JPEG) [8] and Set Partitioning in Hierarchical Trees (SPIHT) [9] image coders. The contributions of this paper are:

- We decouple and quantify linear distortion and noise injection in JPEG and SPIHT coders.
- We introduce a new edge correlation measure to quantify distortion of edges and creation of false edges in compressed SAR images.
- We assess the quality of JPEG and SPIHT image coders when applied to SAR images.

This research was supported by an US National Science Foundation Career Award under grant MIP-9701707.

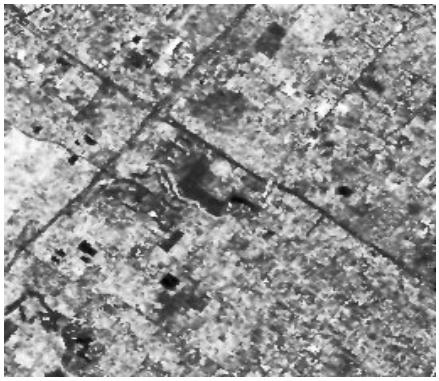

Figure 1: Despeckled SAR image of the city of Houston, Texas, USA.

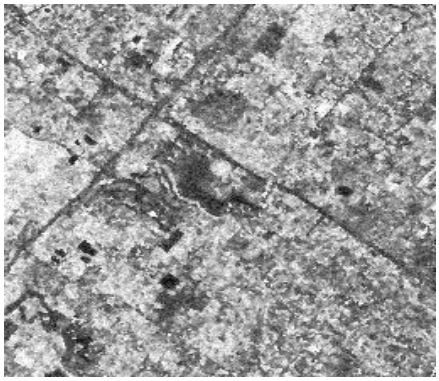

Figure 2: SAR image in Fig. 1 with additive white noise (PSNR is 23.1 dB with respect to Fig. 1).

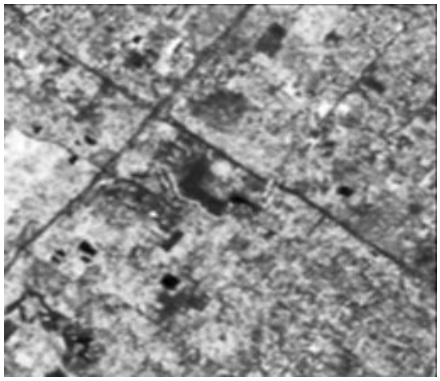

Figure 3: A lowpass filtered version of the SAR image in Fig. 1 (PSNR is 23.1 dB with respect to Fig. 1).

Figure 4: SAR image in Fig. 1 with additive highpass noise (PSNR is 23.1 dB with respect to Fig. 1).

2. BACKGROUND

Fig. 1 shows a despeckled SAR image. Figs. 2–4 are formed by adding white noise to, lowpass filtering, and adding highpass noise to Fig. 1, respectively. Relative to Fig. 1, Figs. 2 and 4 have comparable quality, but Fig. 3 has lower quality than either Fig. 2 and 4. Yet, Figs. 2–4 have the same PSNR (and MSE) values.

Human visual systems respond separately to *frequency distortion* and *noise injection* in still images [6]. We model an image coder as a linear filter plus noise injection (uncorrelated noise), as shown in Fig. 5 [6]. We define a distortion transfer function (DTF) and an SNR measure. The DTF is the deviation of the filter's frequency response $H(\omega_1, \omega_2)$ from an all-pass response: $1 - H(\omega_1, \omega_2)$ [10].

Because we assume human interpretation of the images, we incorporate an HVS model into the quality measures. For simplicity, we use a linear shift-invariant HVS model. We use the model's frequency response, a.k.a. a contrast sensitivity function (CSF), as a perceptual weighting function in the frequency domain [6, 10]. A CSF approximates the visibility of individual Fourier components of an image. Using the lowpass CSF $C(\omega_1, \omega_2)$ in [6, 10], which is plotted in Fig. 6(a), we define a perceptually weighted SNR (WSNR) as

$$\text{WSNR} = 10 \log_{10} \left(\frac{\sum_{\omega_1} \sum_{\omega_2} |X(\omega_1, \omega_2) C(\omega_1, \omega_2)|^2}{\sum_{\omega_1} \sum_{\omega_2} |D(\omega_1, \omega_2) C(\omega_1, \omega_2)|^2} \right)$$

$X(\omega_1, \omega_2)$ and $D(\omega_1, \omega_2)$ are the discrete Fourier transforms of the original and noise images, respectively. The weighted mean of the DTF by the CSF gives a

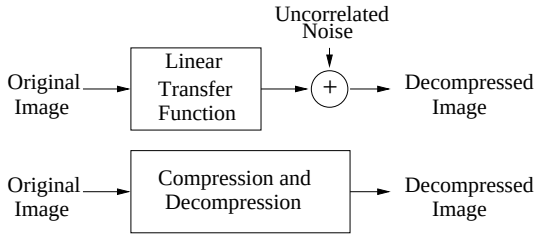

Figure 5: Linear model of compression-decompression.

linear distortion measure (LDM): [10]

$$\text{LDM} = \frac{\sum_{\omega_1}\sum_{\omega_2}|C(\omega_1,\omega_2)||1-H(\omega_1,\omega_2)|}{\sum_{\omega_1}\sum_{\omega_2}|C(\omega_1,\omega_2)|}$$

3. ESTIMATING THE LINEAR FILTER AND NOISE INJECTION

We apply the discrete Fourier Transform (DFT) to subblocks to estimate the linear filter. To reduce false edge effects along the image boundaries, we reflect the 512×512 original and decompressed images in both axes to form 1024×1024 images. We compute the DFT of the 1024×1024 images. Then, we divide the frequency domain into 256 non-overlapping blocks of size 64×64. We assume that the transfer function is constant in each block and estimate its value for each block independently. For each DFT block, we rearrange the pixels into column vectors denoted $\mathbf{x}$ and $\mathbf{y}$ for the original and decompressed images, respectively. Finally, we compute the optimal solution in the least squares sense [11] for $\mathbf{H}$, which is the frequency response of the filter for each block, such that the error vector $\mathbf{e} = \mathbf{y} - \mathbf{H}\mathbf{x}$ is uncorrelated with $\mathbf{x}$:

$$\mathbf{e}^H\mathbf{x} = (\mathbf{y}-\mathbf{H}\mathbf{x})^H\mathbf{x} = 0 \implies \mathbf{H} = \frac{\mathbf{y}^H\mathbf{x}}{\mathbf{x}^H\mathbf{x}}$$

The resulting error vector is the uncorrelated noise.

4. EDGE CORRELATION MEASURE

The noise image is uncorrelated with the original image, but not independent. As a result, nonlinear distortion is included in the uncorrelated noise. Nonlinear distortion, such as blocking artifacts and mosquito noise, is more significant at high compression ratios. Since these artifacts are predominantly high frequency effects, we filter the decompressed images to extract the edge information so that the artifacts are more noticeable and easier to measure. To extract an edge image, we use a 3×3 discrete approximation of a Laplacian operator. The correlation of the edge images is used as a measure of high-frequency distortion which consist primarily of non-linear distortion. An edge image emphasizes terrain boundaries, which are key sources of information in interpreting SAR images. The correlation between edge images of the original and decompressed images measures the degradation of this important information in a SAR image.

5. QUALITY ASSESSMENT

For simulation, we use JPL Spaceborne Imaging Radar C/X Band SAR images [12]. We crop them to 512×512 8-bit grayscale sub-images and compress 7 sub-images using JPEG and SPIHT coders. The images have high-frequency content of rivers, cities, and volcanos, and low-frequency content of oceans and plains.

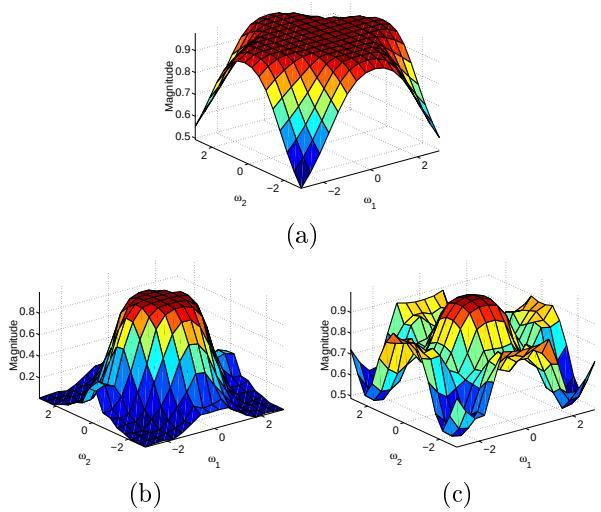

(a) (b) (c)

Figure 6: (a) A Contrast Sensitivity Function of the human visual system, (b) the computed linear model for JPEG at 1.8 bits/pixel, and (c) the computed linear model for SPIHT for 1.8 bits/pixel.

Image	PSNR (dB)	WSNR (dB)	Error corr.	LDM	Edge corr.
without the proposed model					
white noise added	23.1	-	0.0089	-	0.74
highpass noise added	23.1	-	0.0082	-	0.73
linearly distorted	23.1	-	0.5919	-	0.42
with the proposed model					
white noise added	23.1	21.5	1×10^{-6}	0.009	0.74
high-pass noise added	23.1	26.8	5×10^{-8}	0.008	0.73
linearly distorted	44.1	41.0	9×10^{-6}	0.819	0.42

Table 1: Quality measures for images in Figs. 2–4.

Table 1 gives the quality measures for the images in Figs. 2–4. The upper part of Table 1 shows that the residual for the lowpass filtered image in Fig. 3 is highly correlated with the original image in Fig. 1. Therefore, PSNR and MSE measures are not valid for this image. The lower part of Table 1 shows quality measures calculated after decorrelating the error image from the original according to Section 3. After decorrelation, the PSNR value for the lowpass distorted image is higher than that for the other images because no noise has been added to this image. The reason why the PSNR is not infinite is that the estimation of DTF is not perfect. For noisy images, the linear distortion, PSNR, and WSNR are relatively small.

Although the highpass noise added image looks bet-

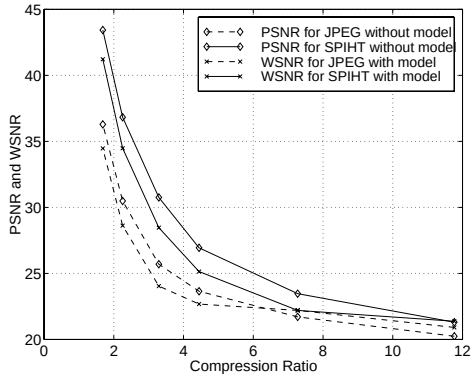

Figure 7: PSNR and WSNR for JPEG and SPIHT coders with and without using the proposed model in Fig. 5.

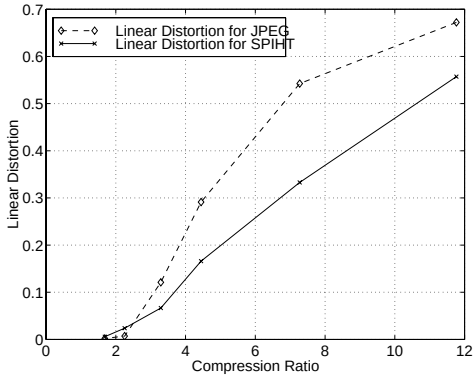

Figure 8: Linear Distortion Measure for Houston.

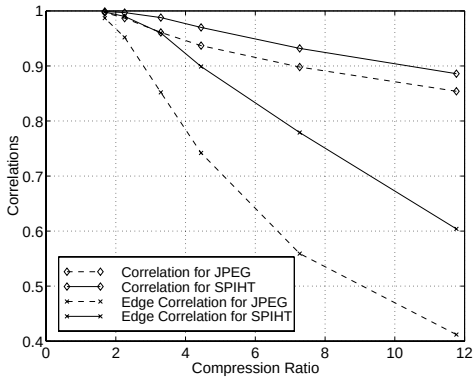

Figure 9: Image Correlation for Houston.

ter than the white noise added image in Figs. 3 and 4, they have the same PSNR. The WSNR, however, is consistent with visual quality. PSNR and WSNR do not measure the absolute quality of the images, but indicate the amount of noise in each image. The edge correlation is lower for the lowpass filtered image since the lowpass distortion operation smoothes the edges.

Figs. 6(b) and 6(c) show the frequency response of the linear models of JPEG and SPIHT coders operating at 1.80 bits/pixel. The linear models capture the lowpass bias in JPEG encoders and the subband decomposition used in SPIHT. The model for SPIHT shows three subband levels with higher frequency bands being quantized to fewer bits.

Figs. 7-9 show rate-distortion curves for the SAR image in Fig. 1. PSNR is higher for SPIHT than JPEG at all compression ratios; WSNR results are closer. At compression ratios above 6, WSNR performance is comparable, as verified by visual inspection, because SPIHT generates more low-frequency noise. The visual effect of the noise is comparable to that of JPEG, even though MSE is lower. As shown in Fig. 8 and expected from the appearance of the linear models in Figs. 6(b) and 6(c), SPIHT introduces less linear distortion than JPEG for compression ratios of 3 and higher.

The correlation between the decompressed and original images is close to one for both compression techniques, with SPIHT being better than JPEG, as shown in Fig. 9. For correlation of edge information, SPIHT outperforms JPEG, which is consistent with the degree of nonlinear distortion observed.

Figs. 10-13 show results for four different images. By judging from PSNR alone in Fig 10, we conclude that SPIHT outperforms JPEG by 7 dB for low and 2 dB for high compression ratios. By using the proposed measures in Figs. 11–13, however, we can quantify noise, linear distortion and edge preservation individually, and compare the techniques for each measure. By comparing Figs. 10 and 11 for low compression ratios, such as 2, the differences between JPEG and SPIHT for both PSNR and WSNR are approximately 7 dB. For the three images in these figures, the differences in the WSNR for JPEG and SPIHT are not as large as the differences in PSNR when the compression ratio is high, e.g. 10:1. At higher compression ratios, linear distortion and edge degradation become significant. If we had two closely performing compression schemes, e.g. less than one dB difference, then PSNR could be misleading because it gives a biased measure that is inconsistent with visual quality.

6. CONCLUSION

Lossy image compression subjects an image to linear distortion, nonlinear distortion, and additive image-independent noise. The human visual system responds to linear distortion and noise injection in still images separately. So, we model the cascade of lossy image compression and decompression as a linear filter followed by additive uncorrelated noise. The uncorrelated noise consists of nonlinear distortion plus addi-

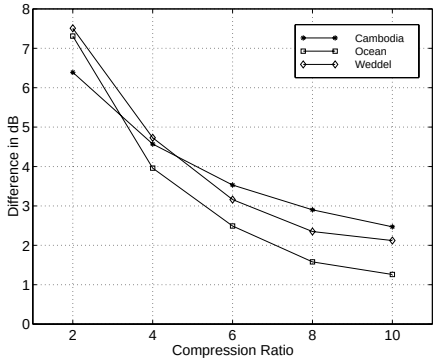

Figure 10: PSNR difference between SPIHT and JPEG for three images.

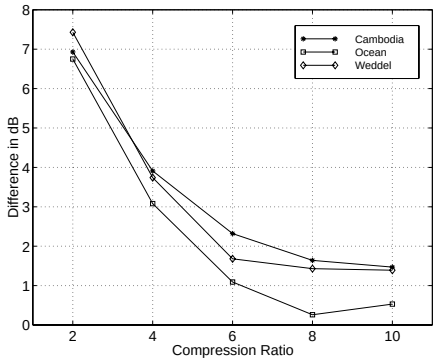

Figure 11: WSNR difference between SPIHT and JPEG for three images.

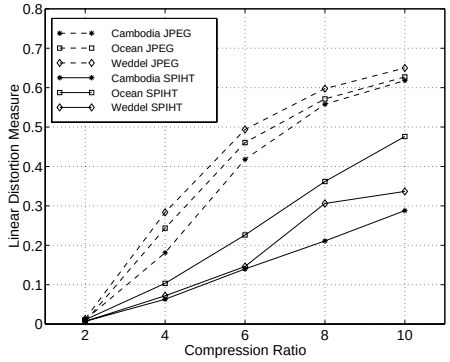

Figure 12: Linear Distortion Measure for SPIHT and JPEG on three images.

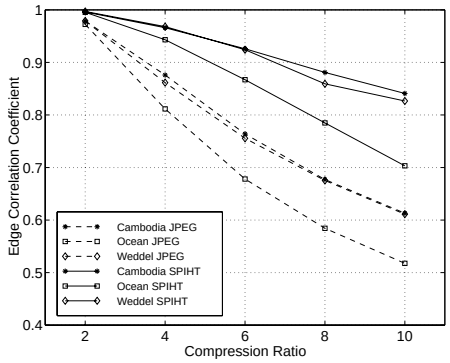

Figure 13: Edge correlation coefficient for SPIHT and JPEG on three images.

tive noise. We introduce a new edge correlation measure that quantifies the nonlinear distortion in which true edges are degraded and false edges are created. We then assess the visual impact of the linear distortion, nonlinear distortion, and additive noise in SAR images compressed by JPEG and SPIHT image coders. We found that SPIHT outperforms JPEG in all three measures.

7. REFERENCES

[1] R. W. Ives, *On the Compression of Synthetic Aperture Radar Imagery*. PhD thesis, Dept. of Electrical and Comp. Eng., Univ. of New Mexico, Albuquerque, NM, May 1998.

[2] M. Dutkicwicz and I. Cumming, "Evaluation of the effect of encoding on SAR data," *Photogrametic Eng. and Remote Sensing*, vol. 60, pp. 895–904, July 1994.

[3] M. Datcu, G. Schwarz, K. Schmidt, and C. Reck, "Quality evaluation of compressed optical and SAR images: JPEG vs. wavelets," in *Proc. Int. Geo. and Remote Sensing Sym.*, vol. 3, pp. 1678–1689, July 1995.

[4] U. Benz, K. Strodl, and A. Moriera, "Comparison of several algorithms for SAR raw data compression," *IEEE Trans. on Geo. and Remote Sensing*, vol. 33, pp. 1266–1276, Sept. 1995.

[5] F. Sakarya, D. Wei, and S. Emek, "An evaluation of SAR image compression techniques," in *Proc. IEEE Int. Conf. on Acoustics, Speech and Signal Proc.*, vol. 4, pp. 2833–2836, Apr. 1997.

[6] T. Kite, *Design and Quality Assessment of Forward and Inverse Error Diffusion Halftoning Algorithms*. PhD thesis, Univ. of Texas at Austin, Austin, TX 78712, Aug. 1998.

[7] G. G. Kuperman and T. D. Penrod, "Evaluation of compressed synthetic aperture radar imagery," in *IEEE National Aero. and Elect. Conf.*, vol. 1, (Dayton, OH), pp. 319–326, May 1994.

[8] W. B. Michelson and J. L. Mitchell, *JPEG Still Image Data Compression Standard*. New York, NY: Van Norstrand Rineholt, 1993.

[9] A. Said and W. A. Pearlman, "A new fast and efficient image codec based on set partitioning in hierarchical trees," *IEEE Trans. on Circuits and Systems for Video Tech.*, vol. 6, pp. 243–250, June 1996.

[10] N. Damera-Venkata, T. D. Kite, W. S. Geisler, B. L. Evans, and A. C. Bovik, "Image quality assessment based on a degradation model," *IEEE Trans. on Image Proc.*, to appear.

[11] S. G. Nash and A. Sofer, *Linear and Nonlinear Programming*. New York, NY: McGraw-Hill, 1996.

[12] "Jet Propulsion Laboratory imaging radar Web site." http://southport.jpl.nasa.gov/.